

Electronic Supporting Information

Evidence of protonation induced intra-molecular metal-to-metal charge transfer in a highly symmetric cyanido bridged {Fe₂Ni₂} molecular square

Prashurya Pritam Mudoi^a, Bipul Sarma^a, Anup Choudhury^a and Nayanmoni Gogoi*^a

a. Department of Chemical Sciences, Tezpur University, Napaam 784028, Sonitpur, Assam, India, Email: ngogoi@tezu.ernet.in

Table of Contents:

Experimental details	S2
Figure S1. Molecular structure of compound 1	S3
Figure S2. FT-IR Spectrum of 1 as KBr disc.....	S4
Figure S3. FT-IR Spectra of 2 and 3 as KBr disc.....	S5
Figure S4. Powder X-ray diffraction pattern of compound 2	S6
Figure S5. Powder X-ray diffraction pattern of compound 3	S7
Figure S6. TGA pattern of compound 2	S8
Figure S7. TGA pattern of compound 3	S9
Figure S8. Variation of $1/\chi_M$ against temperature for compound 3	S10
Figure S9. Field dependence of magnetization of between 0-5 T for 3	S11
Figure S10. Comparison between UV-visible Spectra of 2 in solid state with solution state.....	S12
Figure S11. UV-visible Spectra of $[\text{Fe}(\text{bbp})(\text{CN})_3]^{2-}$ and 3	S13
Figure S12. Comparison between UV-visible Spectra of 3 in solid state with solution state.....	S14
Figure S13. ESI-mass spectrum of 3 in the m/z range 100-2000.....	S15
Figure S14. ESI-mass spectrum of 3 in the m/z range 1500-1800.....	S16
Figure S15. Cyclic voltammogram of 1 and $\text{K}_2\text{Ni}(\text{CN})_4 \cdot \text{H}_2\text{O}$	S17
Figure S16. Cyclic voltammogram of 3	S18
Figure S17. Acid dependence of the $\{\text{Fe}^{\text{III}}(\mu\text{-CN})\text{Ni}^{\text{II}}\}/\{\text{Fe}^{\text{II}}(\mu\text{-CN})\text{Ni}^{\text{III}}\}$ fraction of 3	S19
Figure S18. Base induced UV-visible Spectrum of 3 in DMSO medium.....	S20
Figure S19. Cyclic voltammogram of 3 on acid addition.....	S21
Figure S20. Cyclic voltammogram of 3 on various eq. of acid addition.....	S22
Figure S21. Possible sites for protonation in 3	S23
Table S1. Crystal data and refinement parameters of compound 1 , 2 and 3	S24
Table S2. Selected bond lengths [Å] and bond angles [°] of 1	S25
Table S3. Selected bond lengths [Å] and bond angles [°] of 2	S26
Table S4. Selected bond lengths [Å] and bond angles [°] of 3	S27
Table S5. Comparison of structural properties of cyanido-bridged $\text{Fe}^{\text{III}}\text{-}\text{Ni}^{\text{II}}$ square complexes based on tricyanidoiron (III) building block.....	S28
Table S6. Magnetic parameters for selected square shaped cyanido-bridged $\text{Fe}^{\text{III}}\text{-}\text{Ni}^{\text{II}}$ complexes.....	S29
Table S7. Electrochemical results of complexes 1 , 2 & 3	S30
References	S31

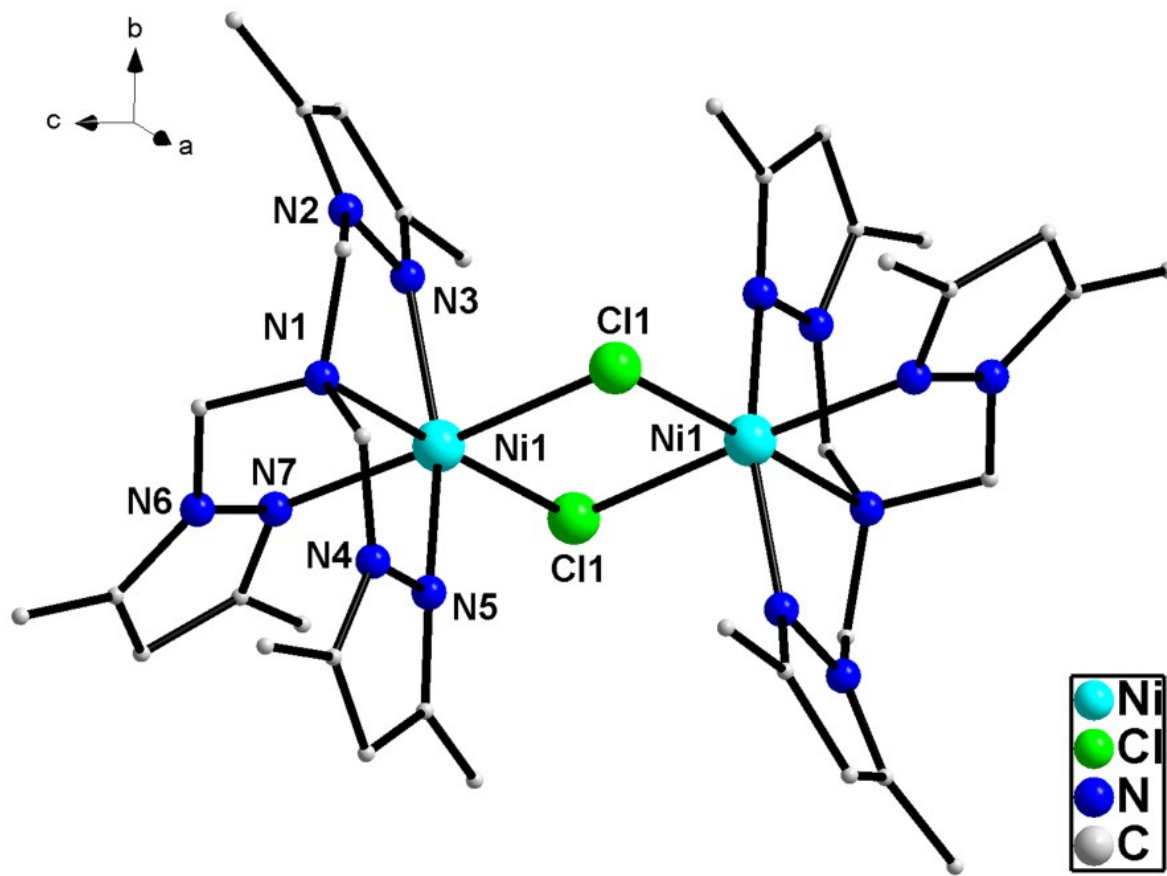


Figure S1: Molecular structure of compound **1**. Counter ion BPh₄ units and aromatic hydrogen atoms are omitted for clarity.

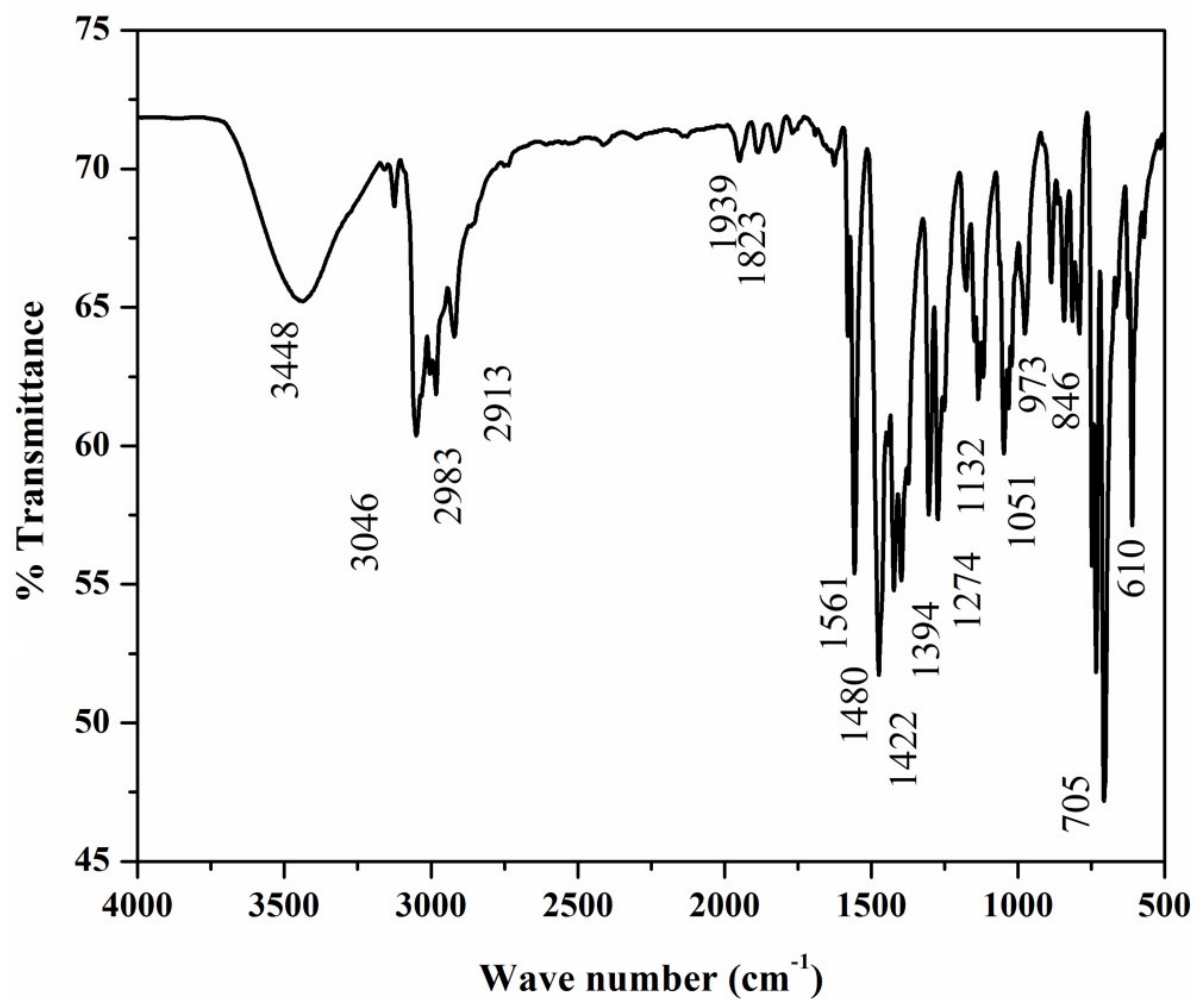


Figure S2: FT-IR spectrum of compound **1** as KBr disc

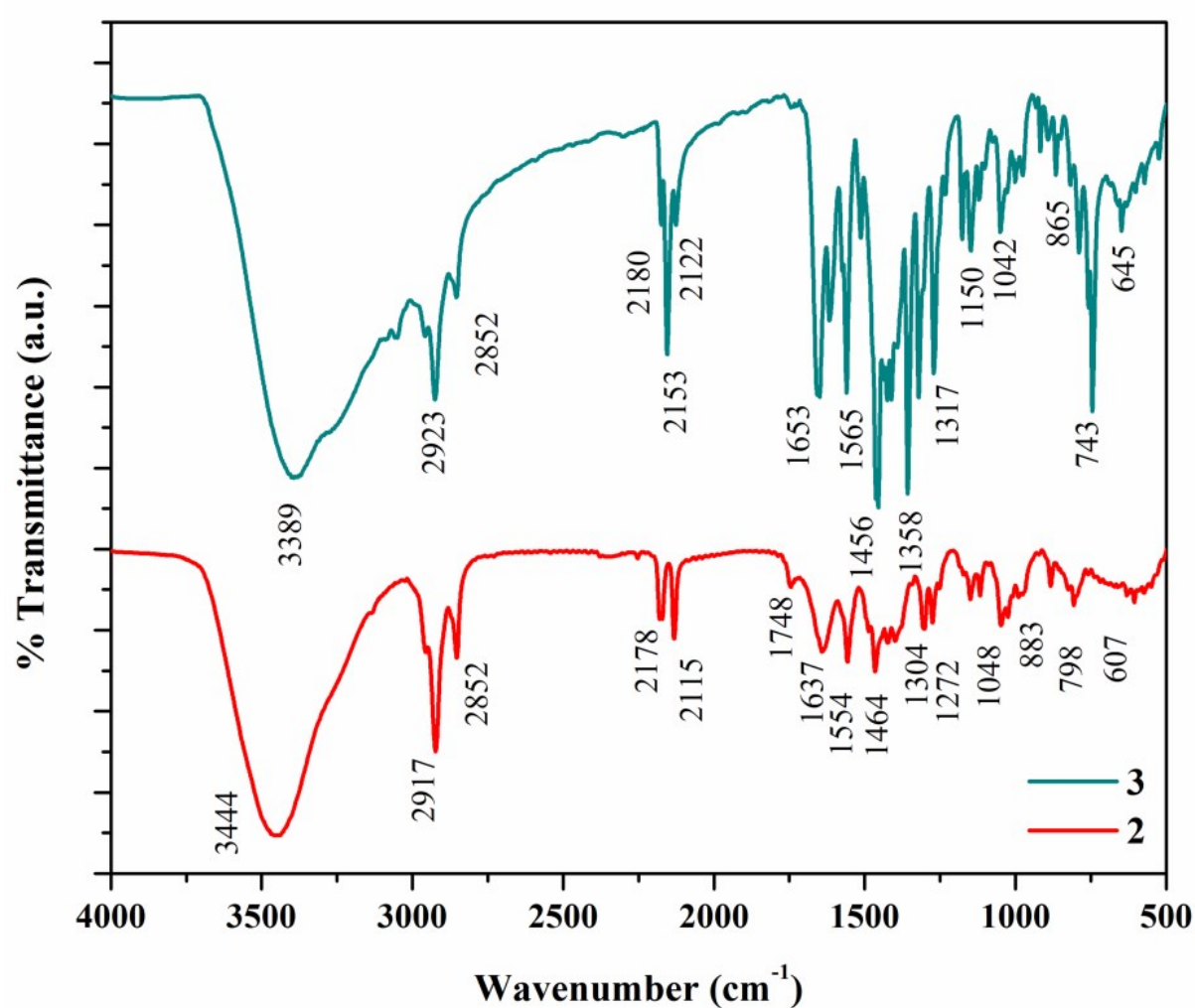


Figure S3: FT-IR spectra of compound **2** and **3** as KBr disc

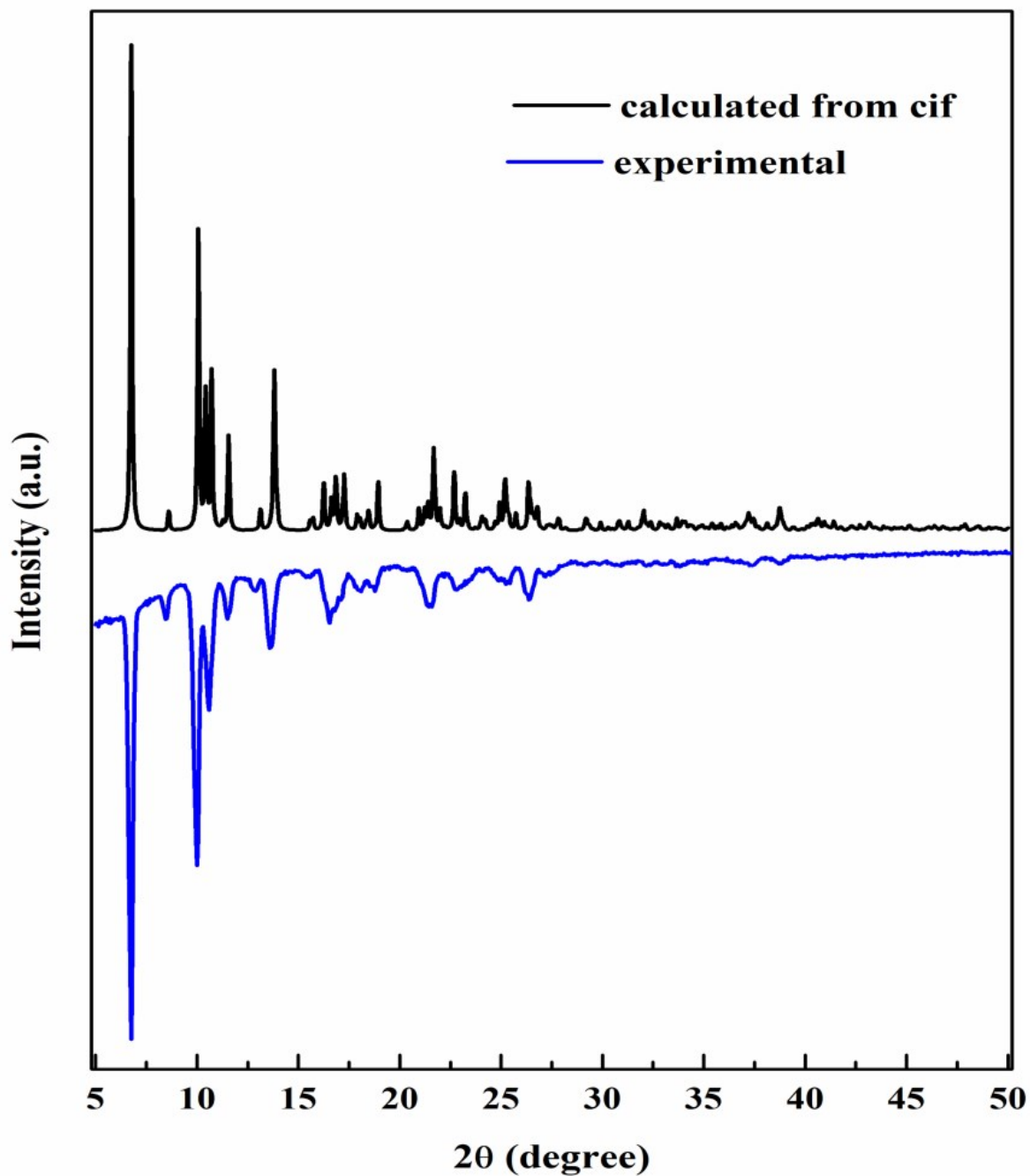


Figure S4: Experimental powder X-ray diffraction (PXRD) pattern of as synthesized **2** (blue solid line) compared with the respective X-ray diffraction pattern calculated from single-crystal X-ray data (black solid line).¹

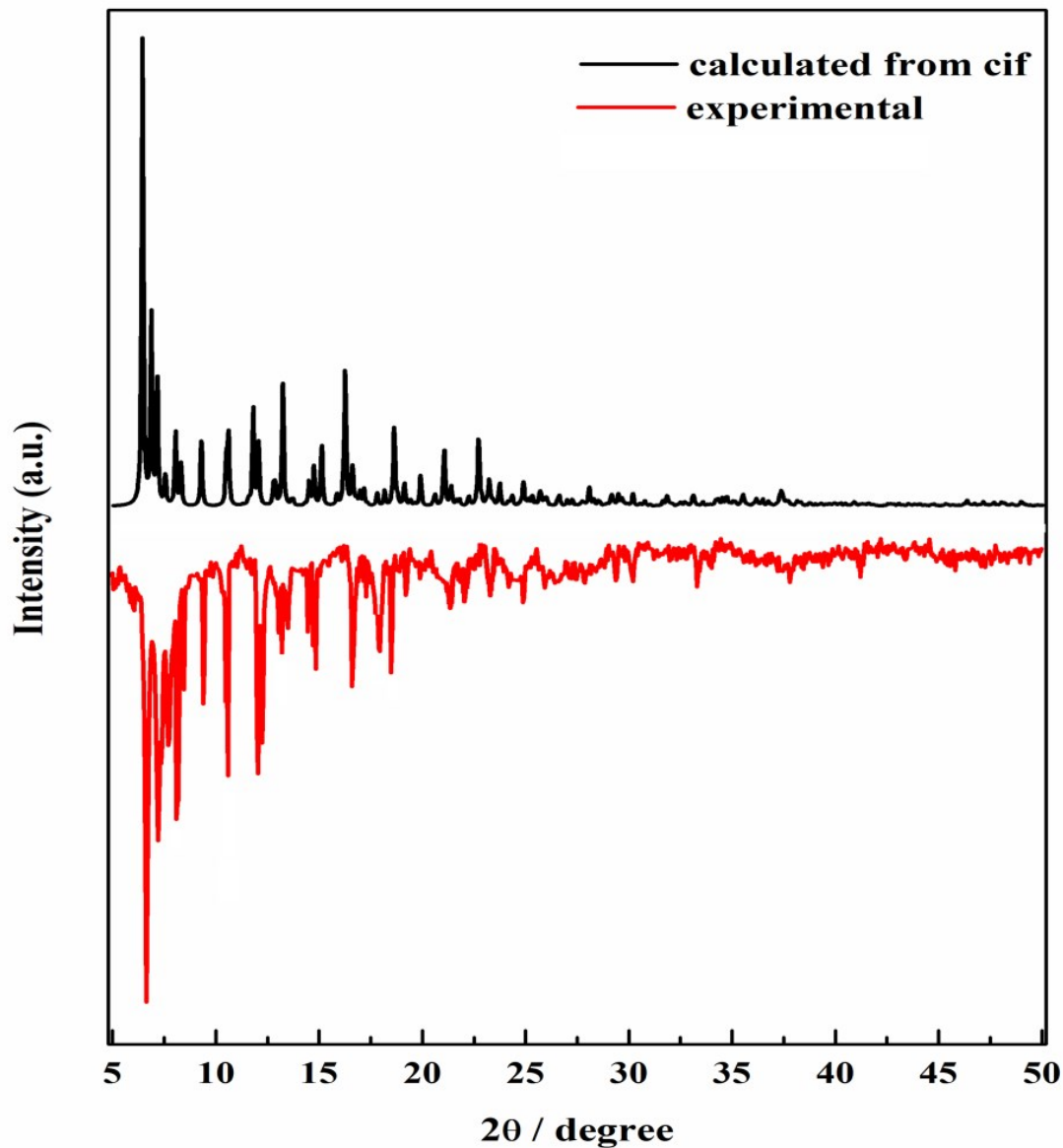


Figure S5: Experimental powder X-ray diffraction pattern of as synthesized **3** (red solid line) compared with the respective X-ray diffraction pattern calculated from single-crystal X-ray data (black solid line).²

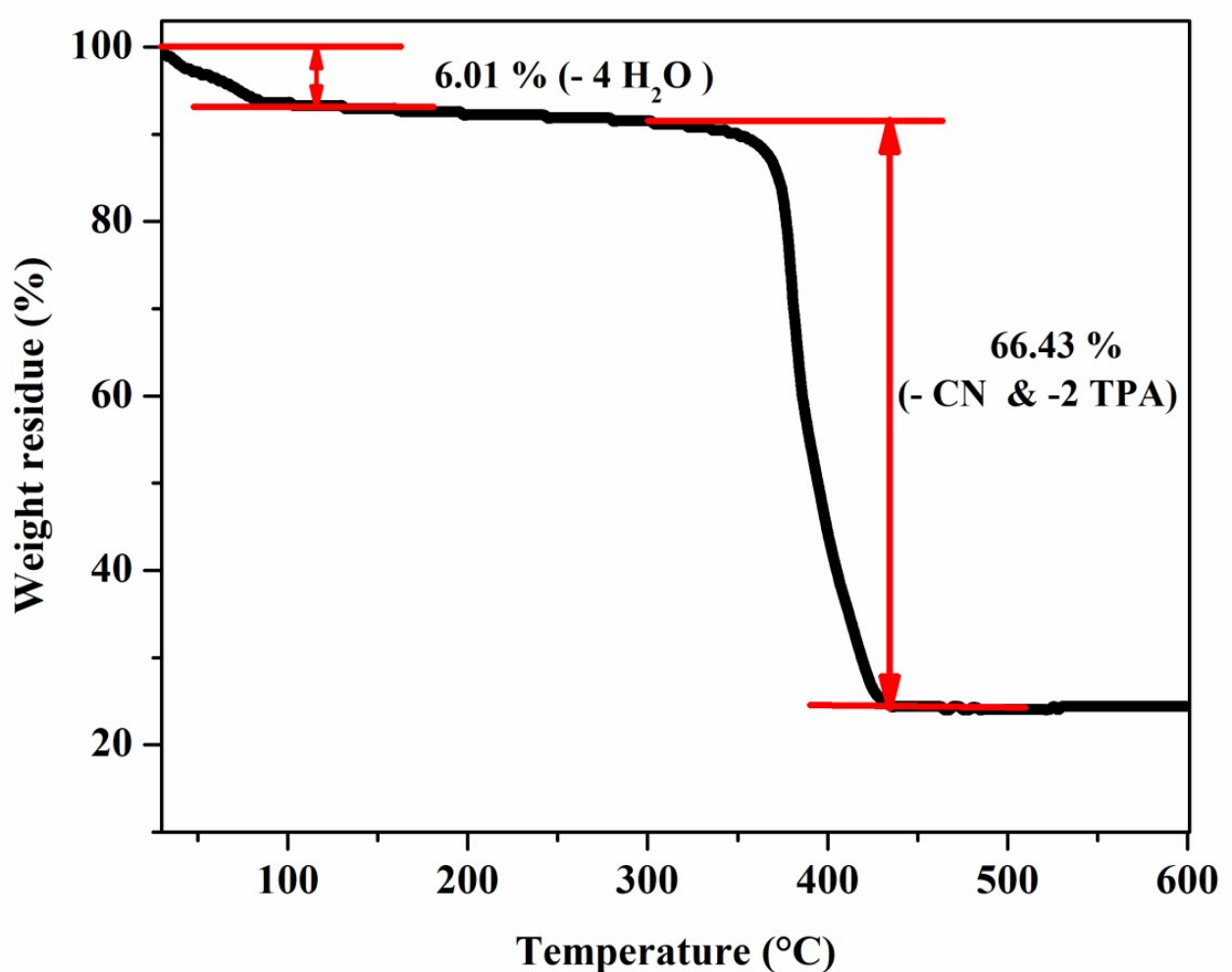


Figure S6: TGA pattern of compound **2** under N₂ atmosphere

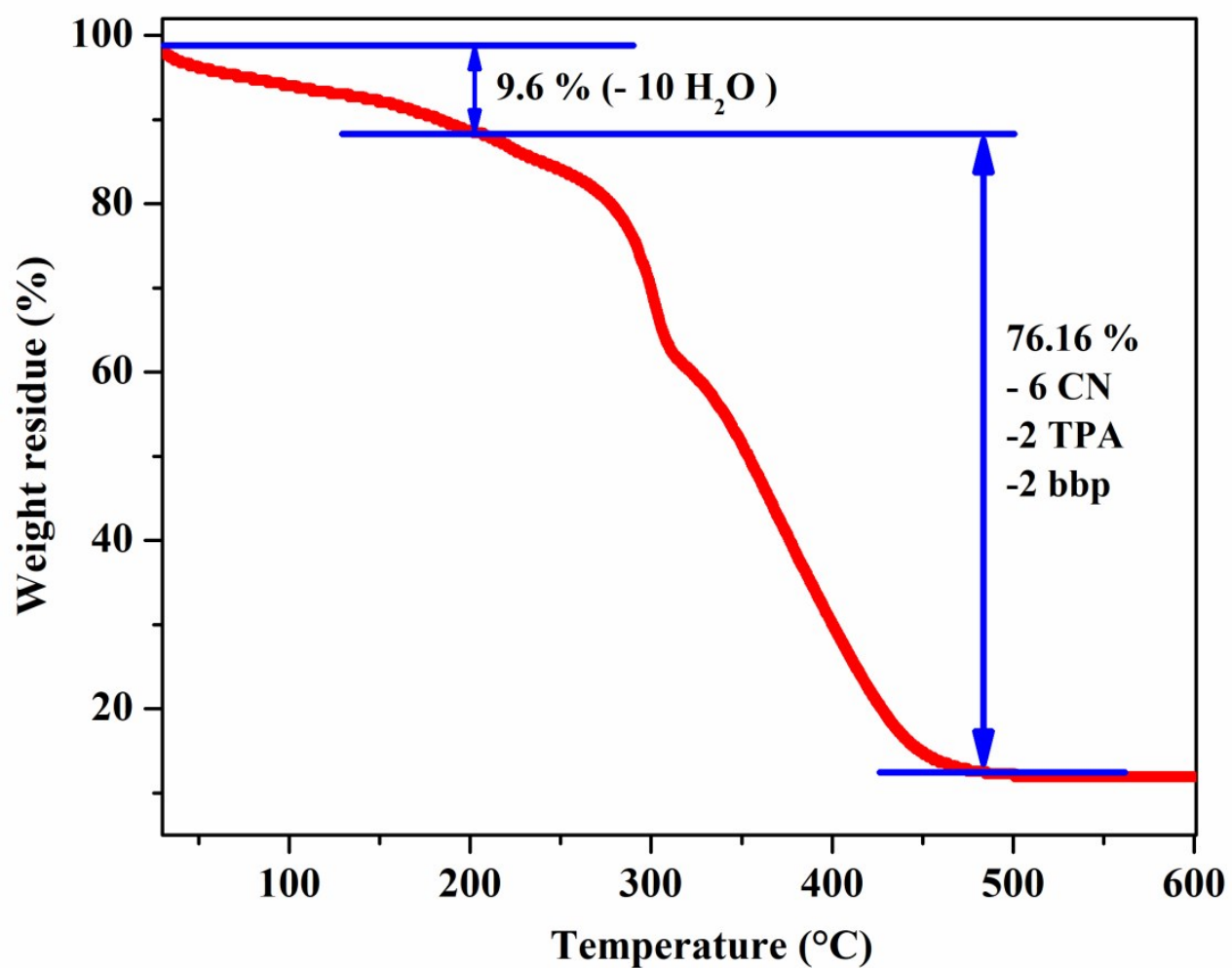


Figure S7: TGA pattern of compound 3.

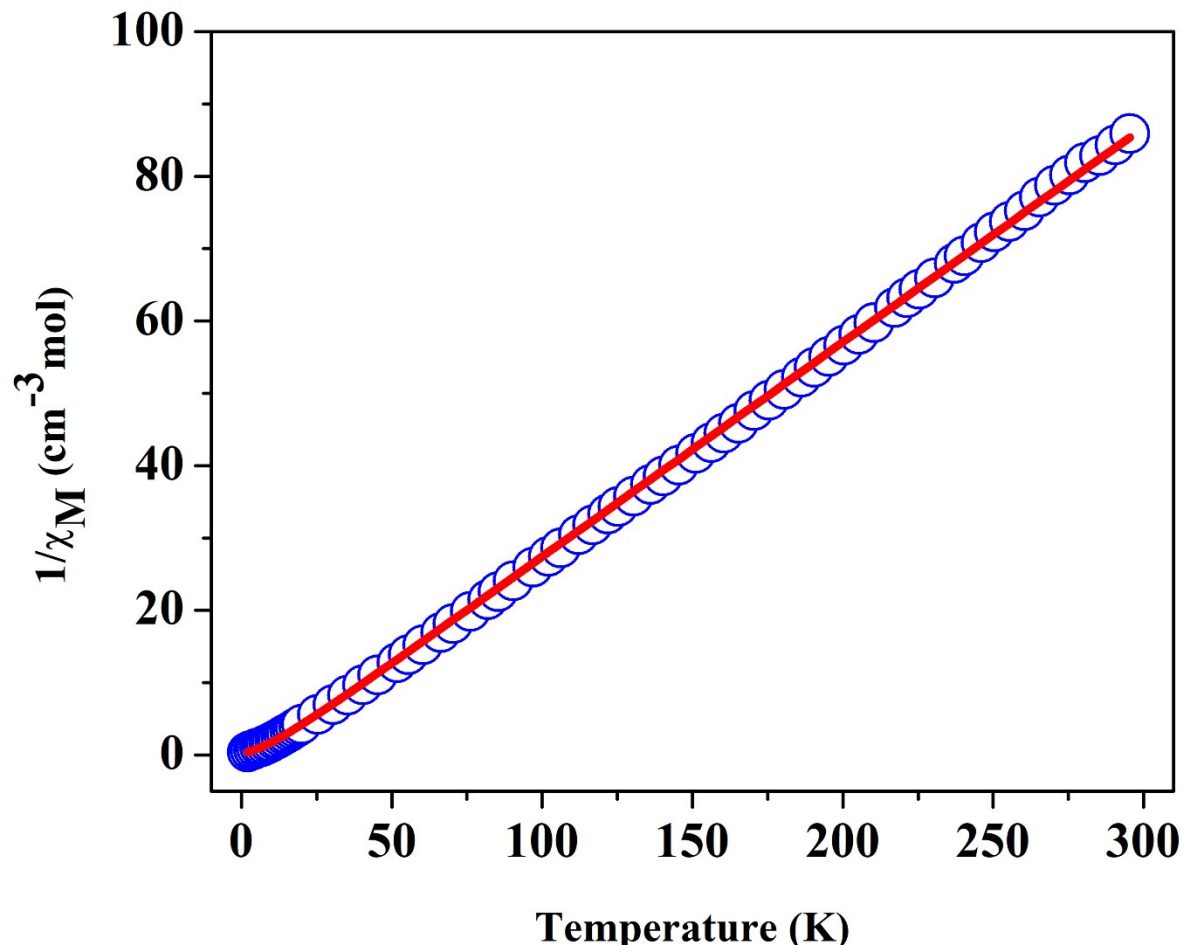


Figure S8: Variation of $1/\chi_M$ against temperature for compound 3

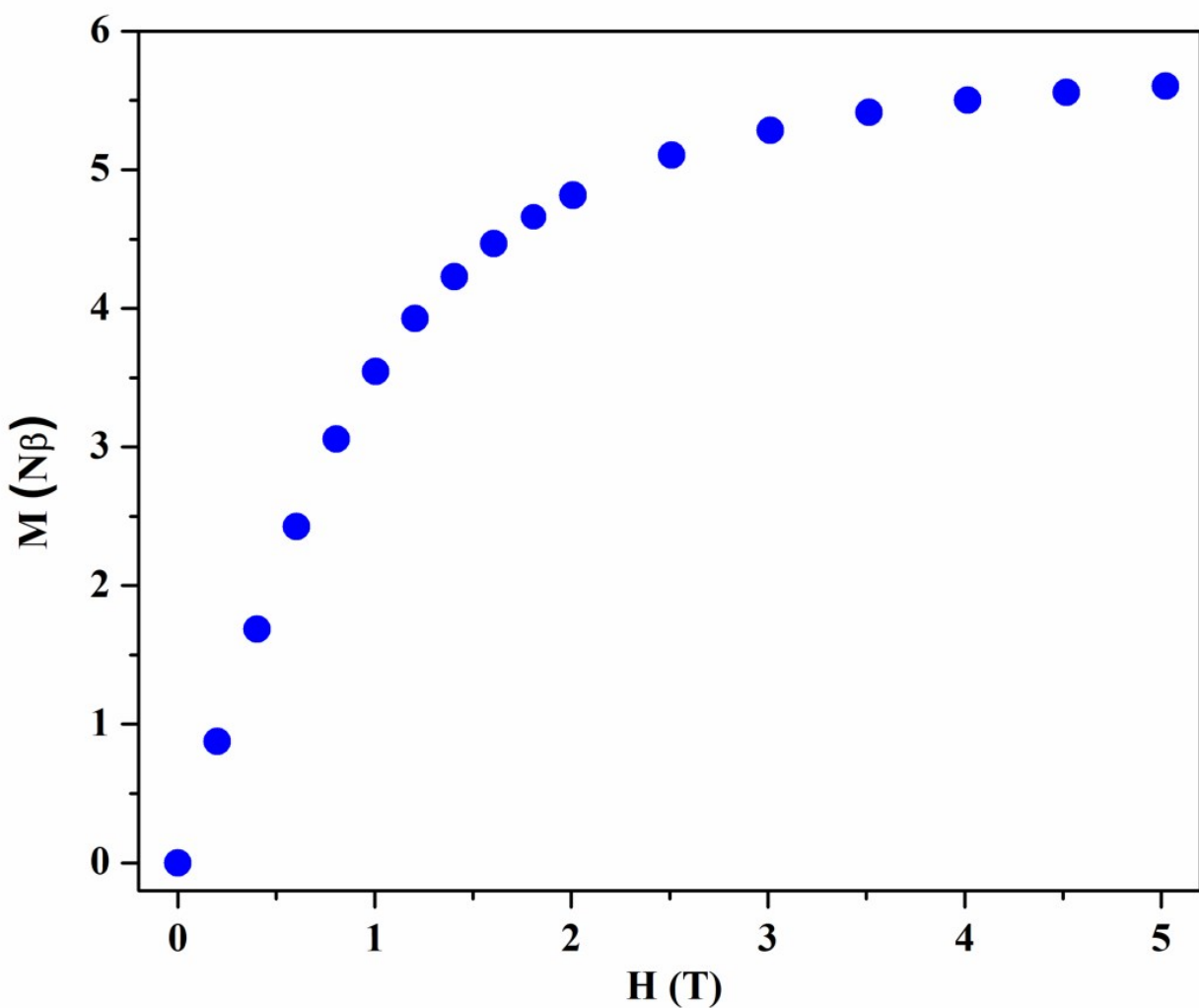


Figure S9: Field dependence of magnetization between 0-5 T for **3** at 2 K.

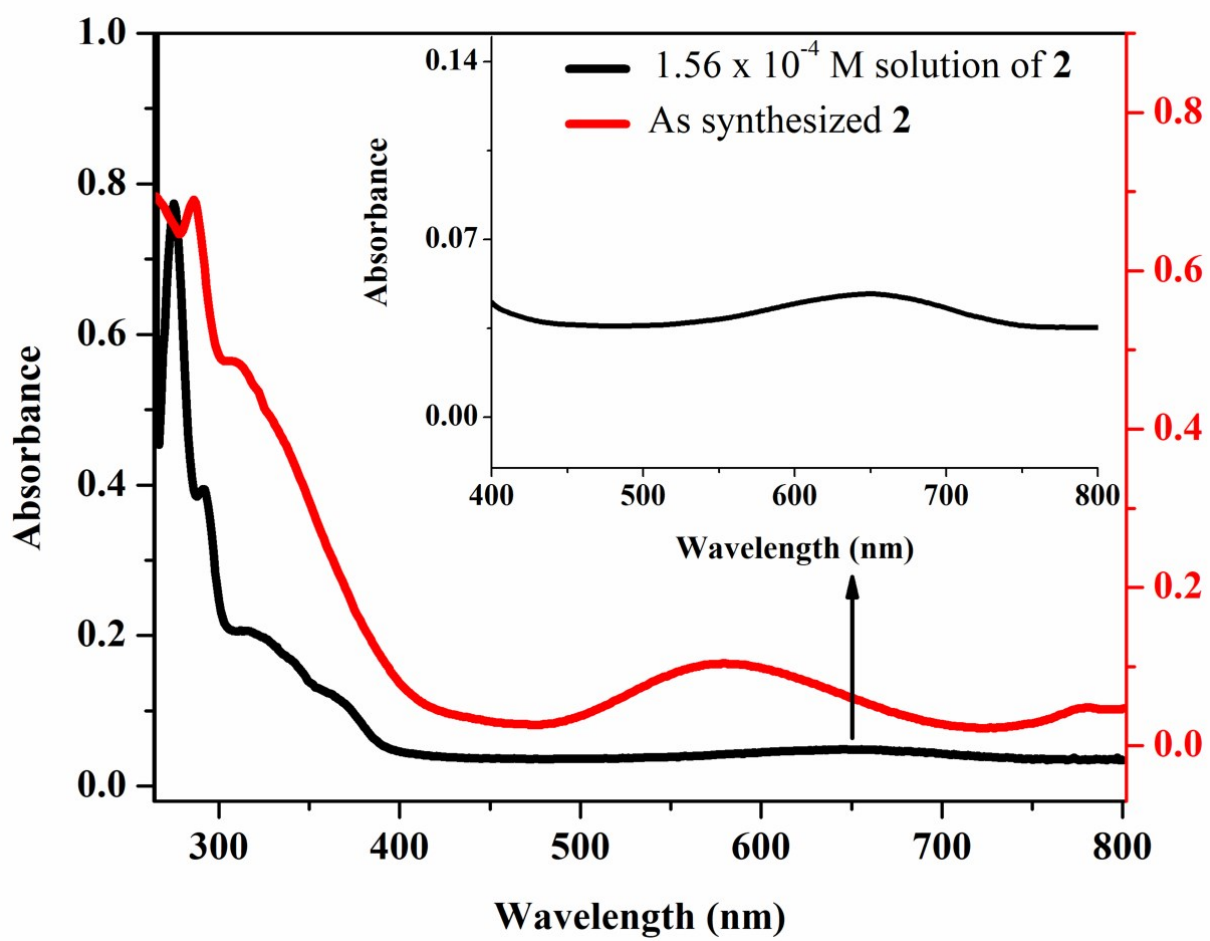


Figure S10: Comparison between UV-visible spectra of as synthesized **2** and 1.56×10^{-4} M solution of **2** in dimethyl formamide recorded at room temperature.

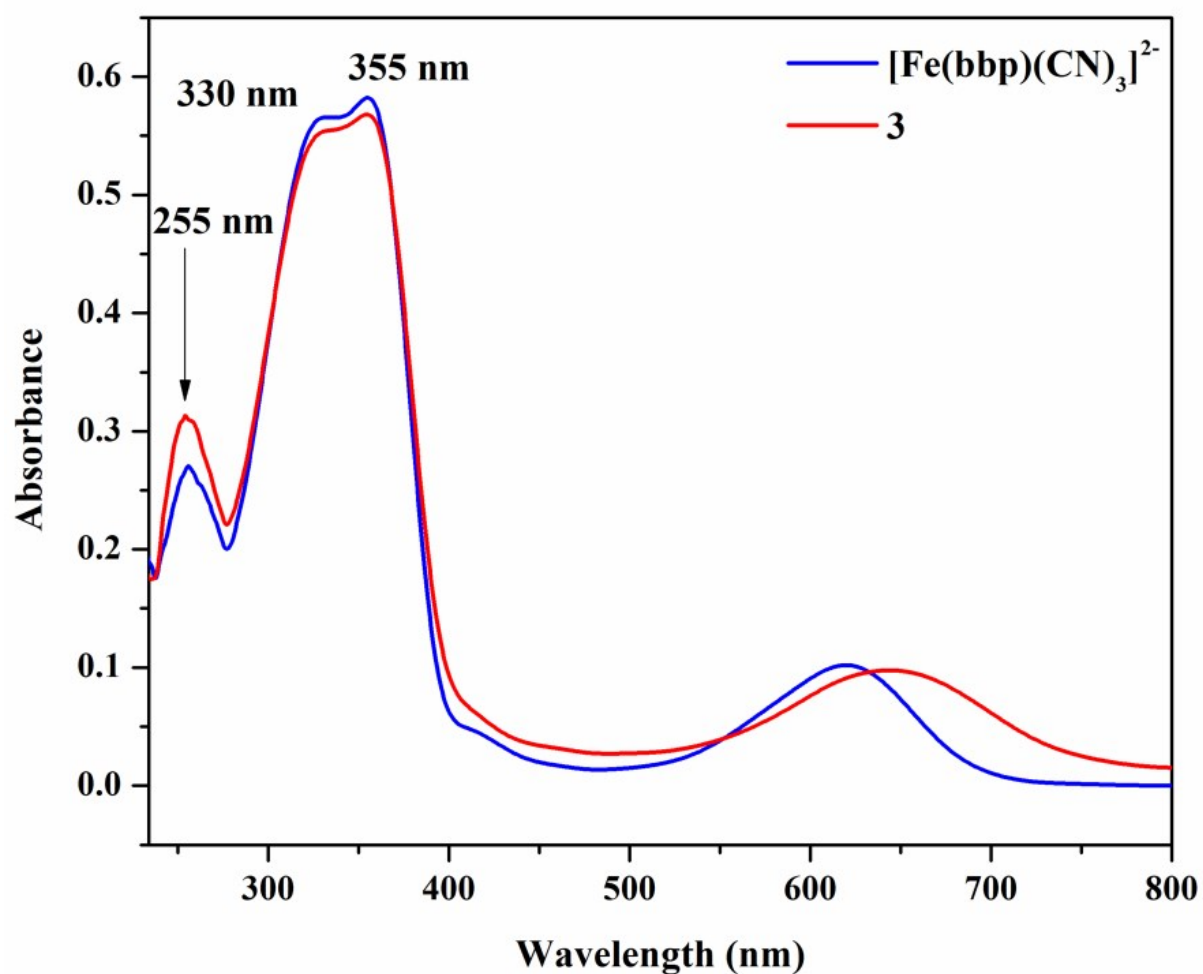


Figure S11: UV-visible spectra of $[\text{Fe}(\text{bbp})(\text{CN})_3]^{2-}$ and 3 in DMSO medium

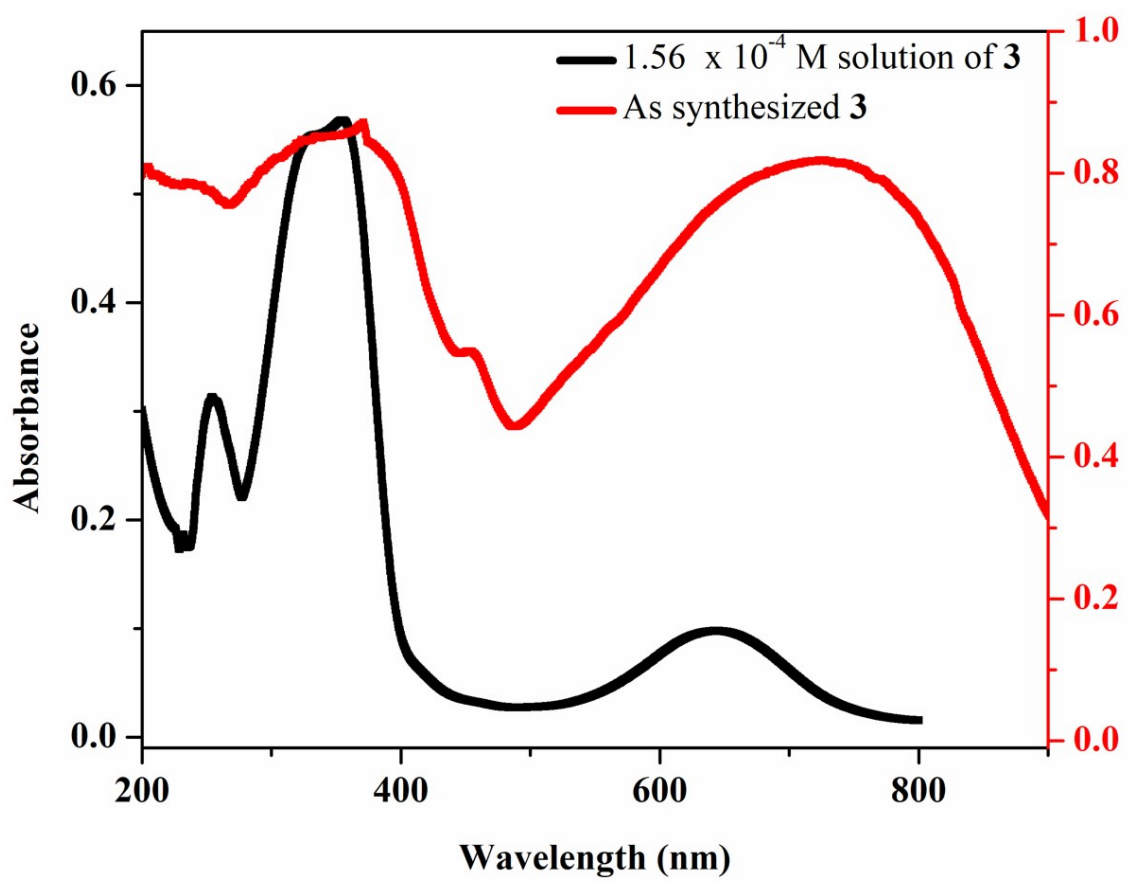


Figure S12: Comparison between UV-visible spectra of as synthesized **3** and 1.56×10^{-4} M solution of **3** in dimethyl sulphoxide recorded at room temperature.

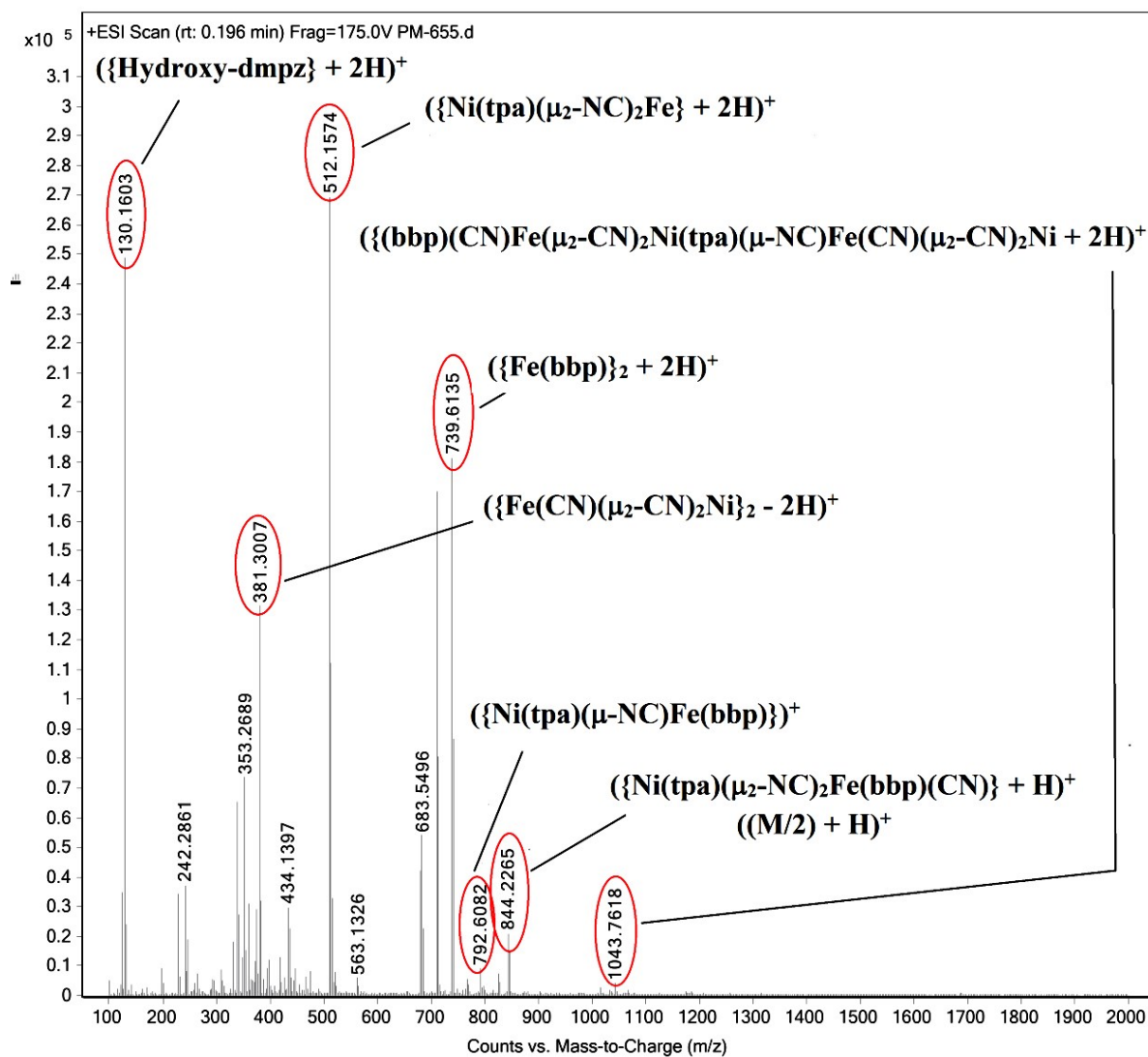


Figure S13: ESI-mass spectrum of **3** in dimethyl sulphoxide in the *m/z* range 100-2000.

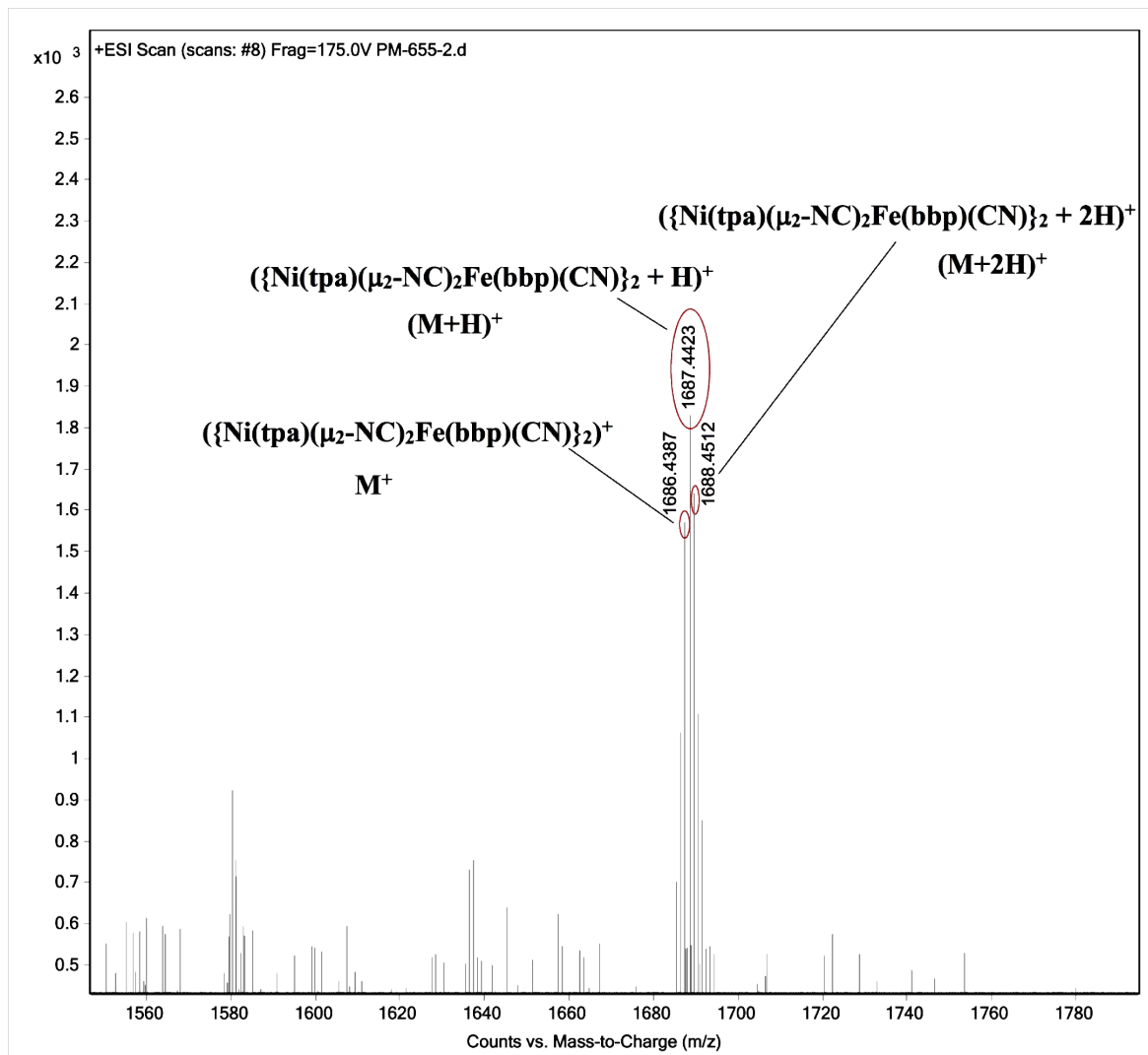


Figure S14: ESI-mass spectrum of **3** in dimethyl sulphoxide in the *m/z* range 1500-1800.

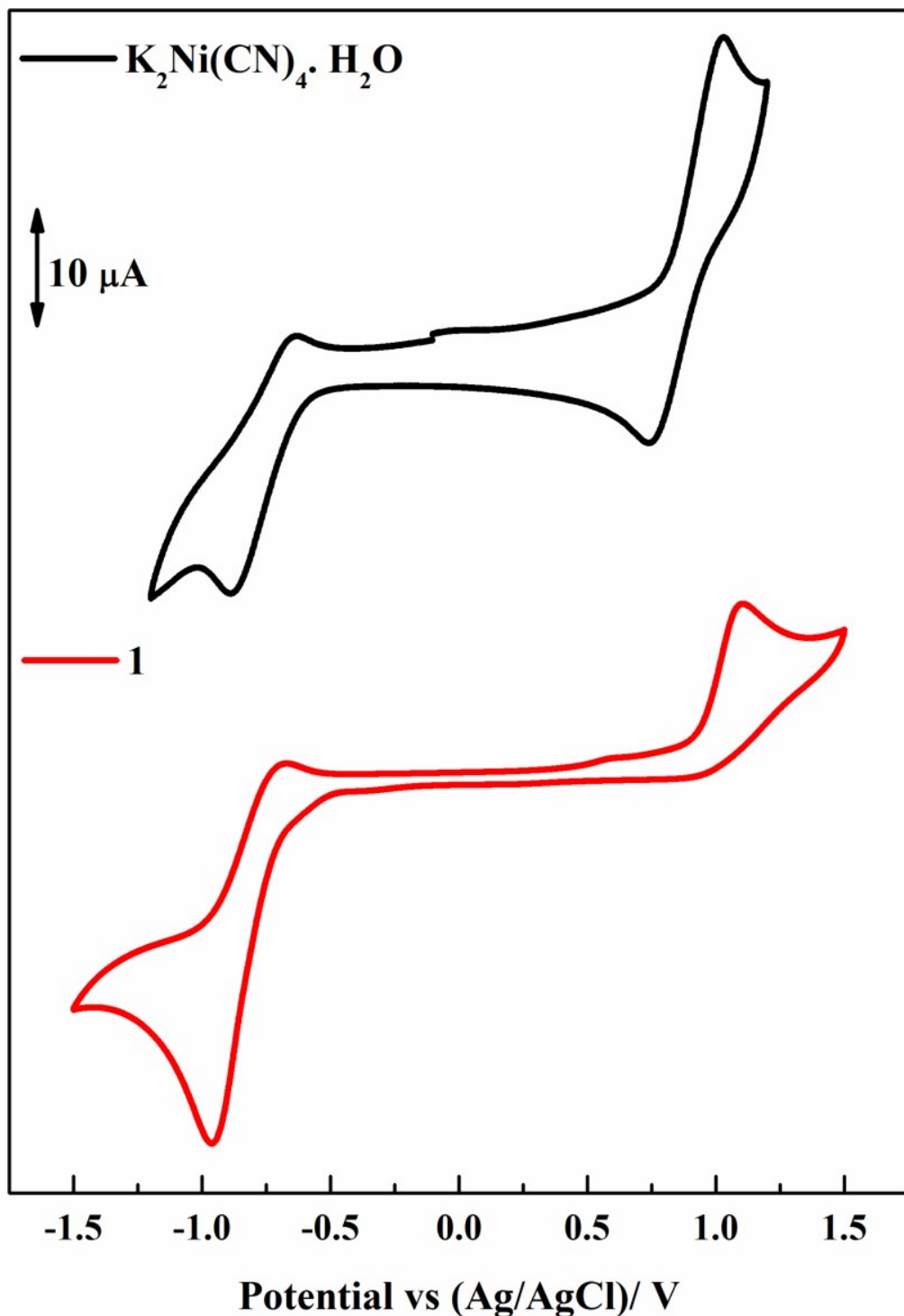


Figure S15: Cyclic voltammogram of **1** and $\text{K}_2\text{Ni}(\text{CN})_4 \cdot \text{H}_2\text{O}$ measured in 0.1 M electrolyte at a scan rate of 100 mV s^{-1}

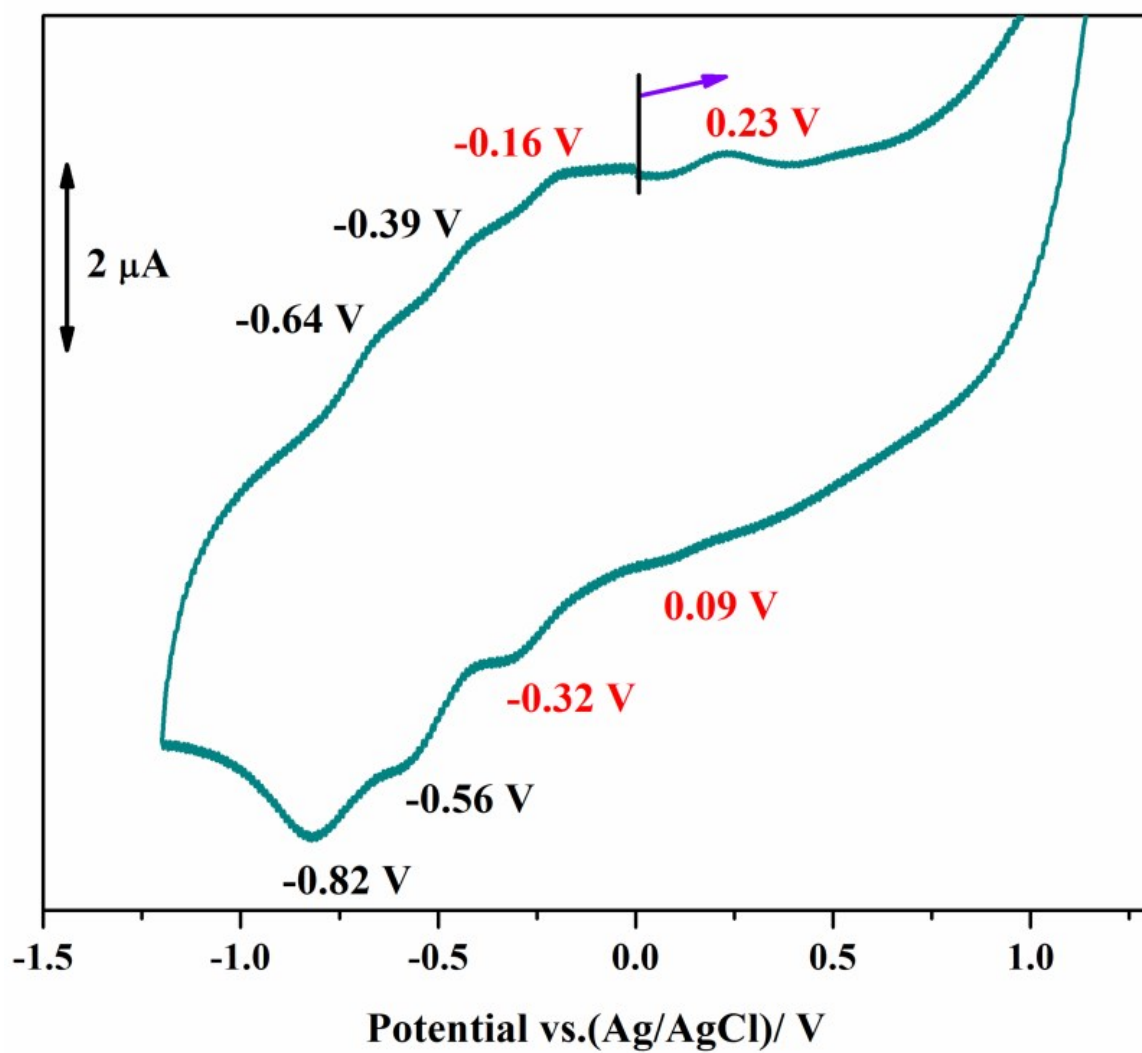


Figure S16: Cyclic voltammogram of **3** measured in 0.1 M electrolyte at a scan rate of 100 mV s⁻¹

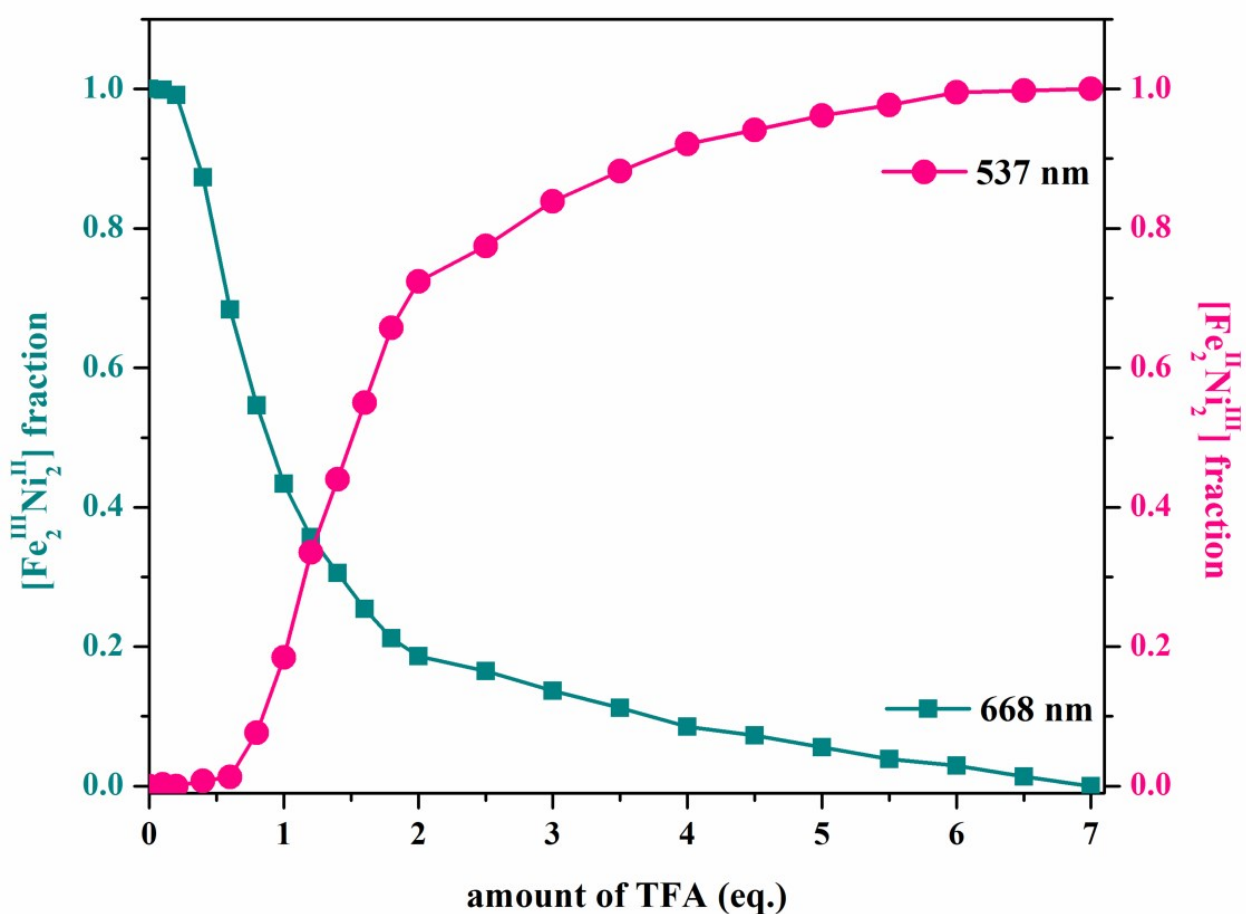


Figure S17: Acid dependence (in equivalent) of the $\{\text{Fe}^{\text{III}}(\mu\text{-CN})\text{Ni}^{\text{II}}\}/\{\text{Fe}^{\text{II}}(\mu\text{-CN})\text{Ni}^{\text{III}}\}$ fraction for **3** estimated from the absorption intensities at the bands 668 nm (blue) and 537 nm (pink).

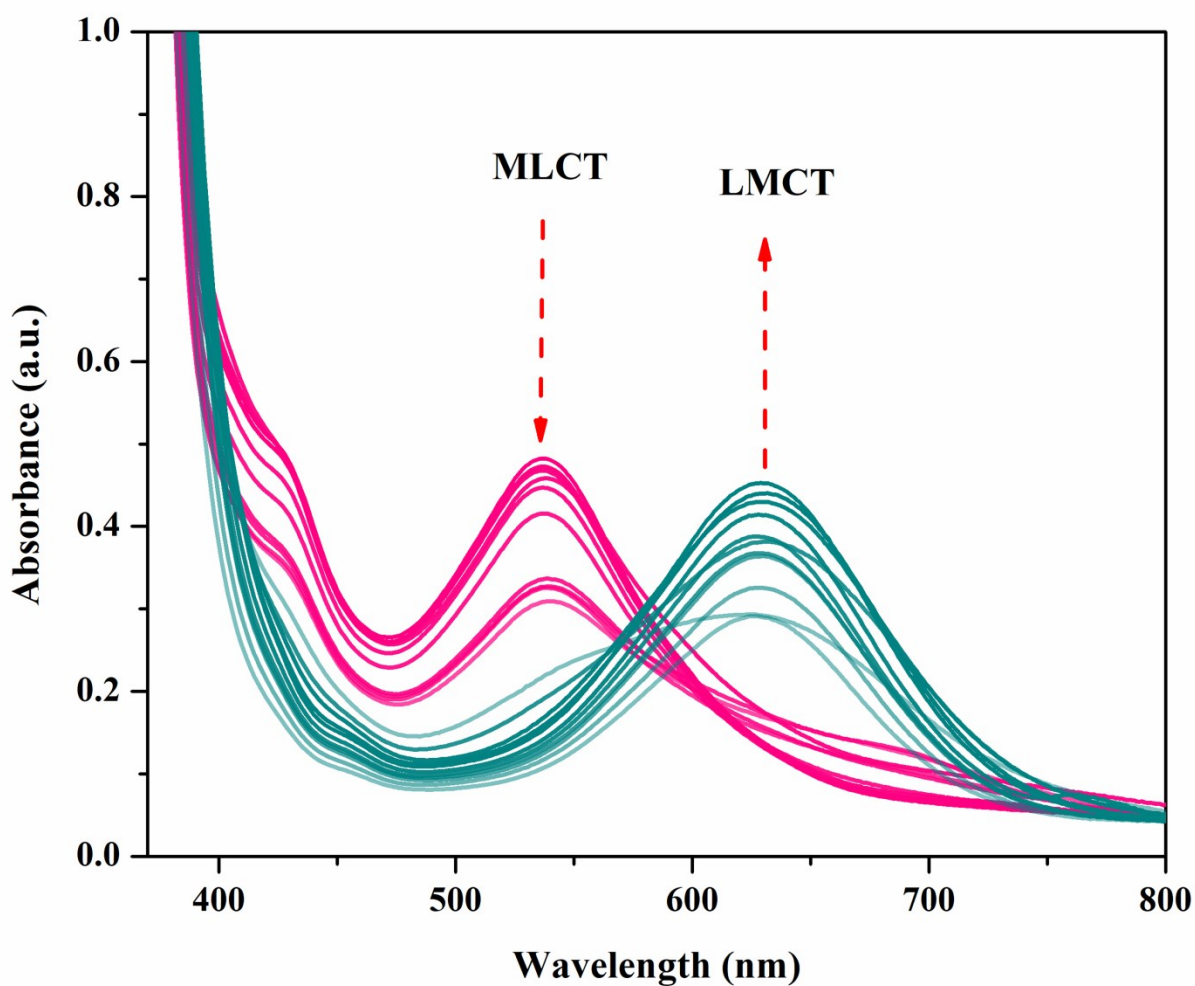


Figure S18: UV-visible spectral evolution of complex **3** upon TEA addition to a TFA added $[\text{Fe}_2\text{Ni}_2]$ in DMSO solution (3.12×10^{-4} M; From purple to blue, the base addition is increasing with an interval of (i) 0.2 eq. up to 1 eq. (ii) 0.4 eq. up to 7.8 eq.

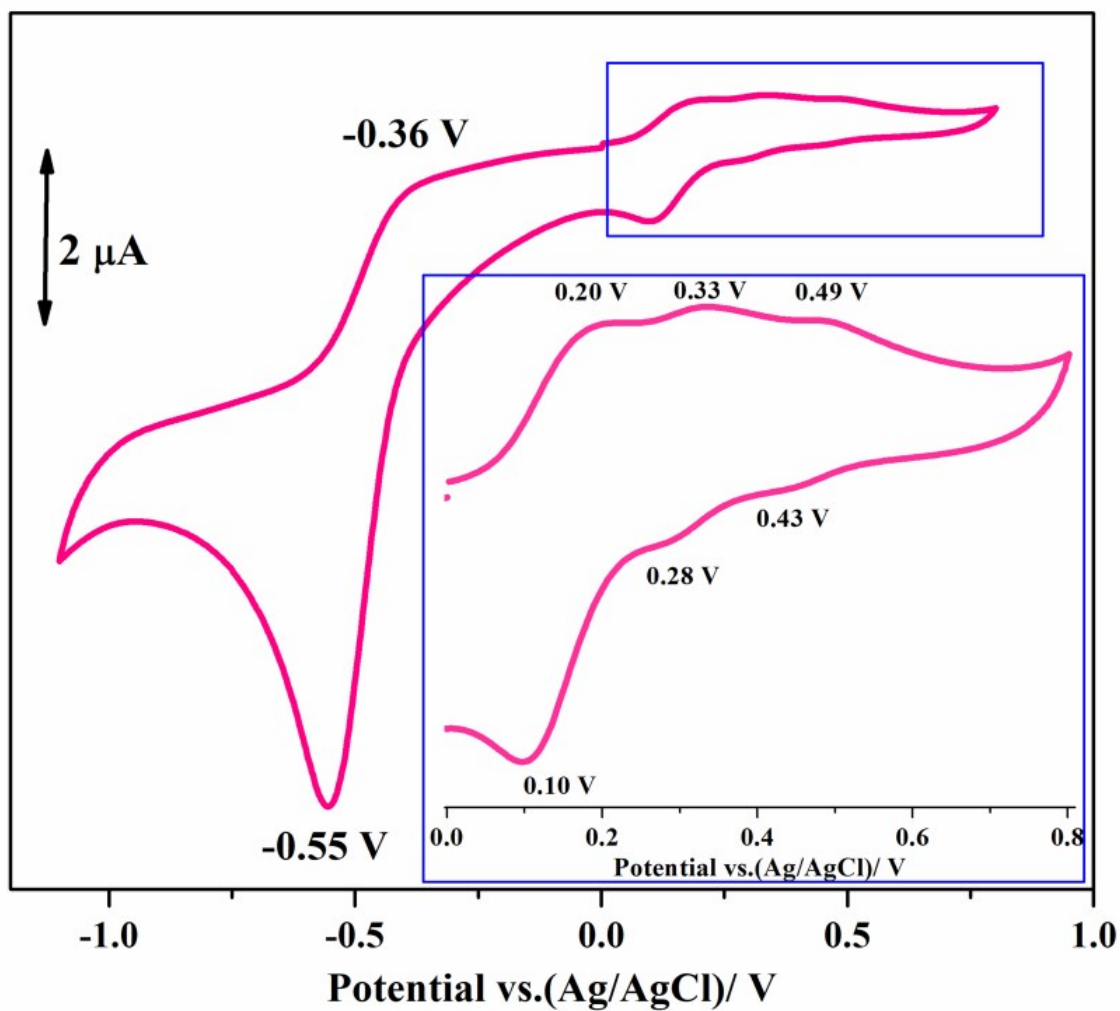


Figure S19: Cyclic voltammogram of **3** after acid addition measured in 0.1 M electrolyte at a scan rate of 100 mV s⁻¹.

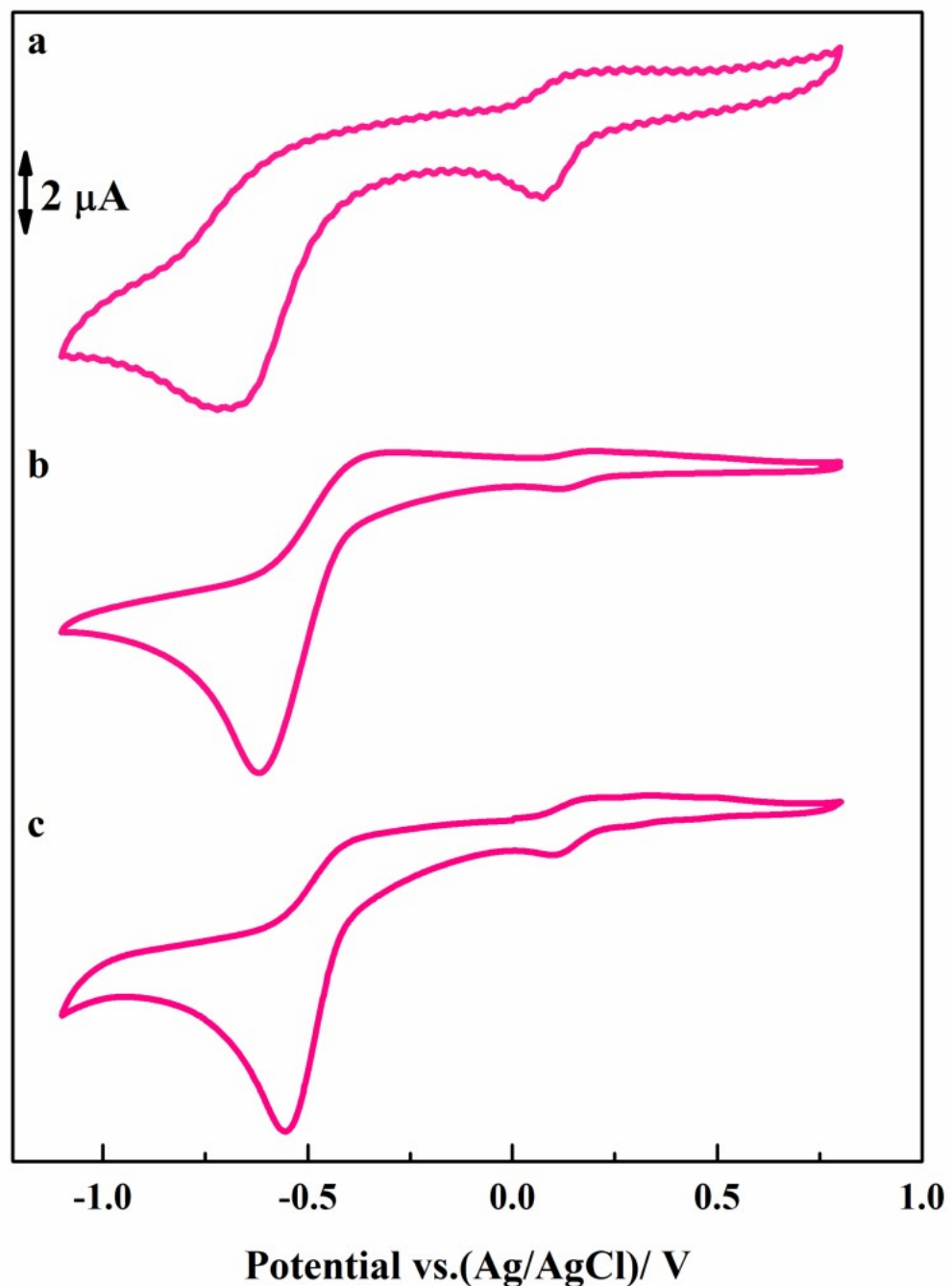


Figure S20: Cyclic voltammogram of **3** after acid addition measured at a scan rate of 100 mV s⁻¹. Cyclic voltammogram is collected after a) 4.2 eq.; b) 6.2 eq. and c) 8.2 eq. of TFA addition.

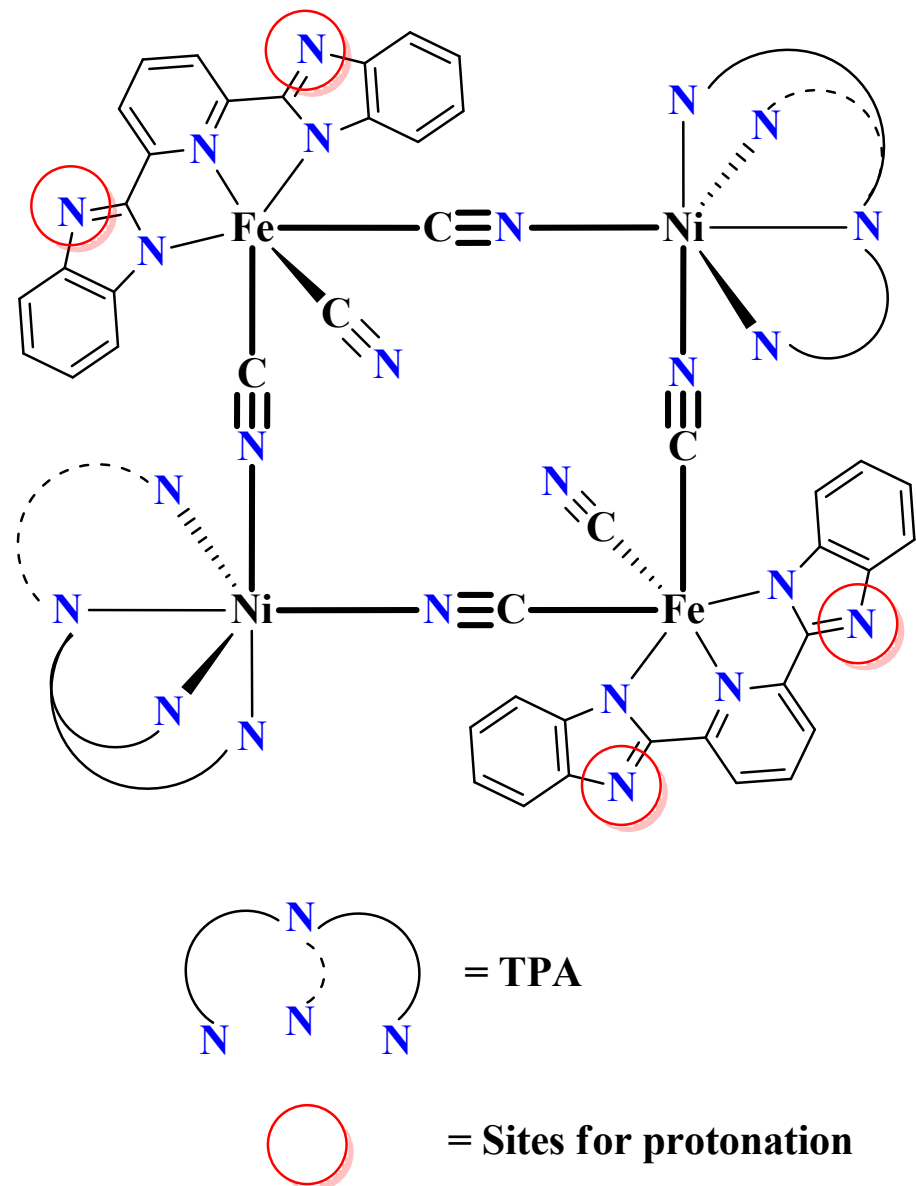


Figure S21: Possible sites for protonation in **3**

Table S1: Crystal data and refinement parameters of compound **1-3**

Compound	1	2	3
CCDC	2020458	1959339	1959340
Empirical formula	C ₈₄ H ₉₄ B ₂ Cl ₂ N ₁₄ Ni ₂	C ₄₄ H ₆₂ N ₂₂ Ni ₄ O ₄	C ₈₀ H ₉₆ Fe ₂ N ₃₀ Ni ₂ O ₁₀
Formula weight	1509.67	1197.88	1866.89
Temperature/K	296	100	100
Crystal system	Triclinic	Monoclinic	Monoclinic
Space group	P ⁻ 1	P 2 ₁ /c	C 2/c
a/Å	10.5897(5)	8.473(11)	28.33(10)
b/Å	11.6576(5)	20.53(3)	13.73(4)
c/Å	17.2621(7)	17.43(2)	26.51(8)
α/°	77.761(2)	90	90
β/°	77.184(2)	103.32(15)	105.62(6)
γ/°	87.782(2)	90	90
Volume/ Å ³	2030.62(16)	2950(7)	9931(54)
Z	1	2	4
Density (calc), mg/m ³	1.235	1.339	1.246
μ/ mm ⁻¹	0.582	1.314	0.725
F(000)	796	1232	3880
Crystal size, mm ³	0.36 x 0.18 x 0.09	0.26 x 0.21 x 0.13	0.16 x 0.12 x 0.08
Theta range for data collection	2.377 to 28.000°	2.319 to 27.000°	2.159 to 20.832°
Reflections collected	60784	79489	56669
Independent reflections	9771	6392	5152
Completeness to theta	99.9 %	99.0 %	98.9 %
Data/restraints/parameters	9771 / 0 / 472	6392 / 0 / 335	5152 / 12 / 601
Goodness-of-fit on F ²	0.940	1.021	0.924
Final R indeces [I>=2σ(I)]	R1 = 0.0418, wR2 = 0.1244	R1 = 0.0561, wR2 = 0.1394	R1 = 0.0804, wR2 = 0.1814
R indices (all data)	R1 = 0.0708, wR2 = 0.1489	R1 = 0.1062, wR2 = 0.1646	R1 = 0.1942, wR2 = 0.2414

Table S2: Selected bond lengths [\AA] and bond angles [$^\circ$] of **1**

Bond Length [\AA]		Bond angles [$^\circ$]	
Ni(1)-N(1)	2.1669(17)	N(3)-Ni(1)-N(5)	158.59(8)
Ni(1)-N(3)	2.0792(18)	N(3)-Ni(1)-N(7)	91.64(7)
Ni(1)-N(5)	2.1170(18)	N(5)-Ni(1)-N(7)	85.50(7)
Ni(1)-N(7)	2.1310(18)	N(3)-Ni(1)-N(1)	79.84(7)
Ni(1)-Cl(1)	2.4951(6)	N(5)-Ni(1)-N(1)	78.75(6)
Ni(1)-Cl(1)#1	2.3499(6)	N(7)-Ni(1)-N(1)	81.38(7)

Table S3: Selected bond lengths [\AA] and bond angles [$^\circ$] of **2**

Bond Length [\AA]		Bond angles [$^\circ$]	
Ni(1)-N(1)	2.178(4)	Ni(1)-N(8)-C(19)	164.9(3)
Ni(1)-N(3)	2.087(4)	Ni(1)-N(9)-C(20)	166.3(3)
Ni(1)-N(5)	2.130(5)	Ni(2)-C(21)-N(10)	178.4(5)
Ni(1)-N(7)	2.162(4)	Ni(2)-C(22)-N(12)	176.6(4)
Ni(1)-N(8)	2.028(5)	N(8)-Ni(1)-N(9)	89.85(15)
Ni(1)-N(9)	2.084(4)	C(19)-Ni(2)-C(20)	91.16(18)

Table S4: Selected bond lengths [\AA] and bond angles [$^\circ$] of **3**

Bond Length [\AA]		Bond angles [$^\circ$]	
Ni(01)-N(1)	2.196(10)	N(1)-Ni(01)-N(3)	79.1(4)
Ni(01)-N(3)	2.141(11)	N(1)-Ni(01)-N(5)	78.4(4)
Ni(01)-N(5)	2.105(11)	N(1)-Ni(01)-N(7)	79.5(4)
Ni(01)-N(7)	2.119(10)	N(1)-Ni(01)-N(140)	92.2(4)
Ni(01)-N(13)	2.003(11)	C(38)-N(13)-Ni(01)	174.2(9)
Fe(02)-N(8)	1.958(10)	C(39)-N(140)-Ni(01)	176.3(9)
Fe(02)-N(9)	1.983(11)	N(8)-Fe(02)-C(38)	90.0(4)
Fe(02)-N(11)	1.979(11)	N(9)-Fe(02)-C(38)	87.6(5)
Fe(02)-C(38)	1.980(14)	N(11)-Fe(02)-C(38)	91.2(4)
Fe(02)#1-C(39)	1.958(15)	C(40)-Fe(02)-C(38)	177.4(5)
Fe(02)-C(40)	1.967(15)	C(39)#1-Fe(02)-C(38)	91.9(5)

Symmetry transformations used to generate equivalent atoms: #1 -x+3/2,-y+1/2,-z+1 #2 -x+2,y,-z+3/2

Table S5: Comparison of structural properties of cyano-bridged Fe^{III}–Ni^{II} square complexes based on tricyanidoiron (III) building block

Compounds	Fe···Ni(Å)	N-Ni-N(°)	C-Fe-C(°)	Reference
[Fe(bbp)(CN) ₃ Ni(tpa)] ₂	5.163-5.172	90.16	91.87	This work
[(Tp)Fe(CN) ₃ Ni(tren)] ₂ (ClO ₄) ₂	5.042-5.156	91.40	86.80	26
[(Tp)Fe(CN) ₃ Ni(bipy) ₂] ₂ [(Tp)Fe(CN) ₃] ₂	5.090-5.099	90.92	87.90	26
[Fe(bbp)(CN) ₃ Ni(tren)] ₂	5.046-5.156	92.10	86.49	22
[(Tp*)Fe ^{III} (CN) ₃ Ni(4-Clbpy) ₂] ₂	5.063-5.085	90.32	87.86	32
[(Tp*)Fe ^{III} (CN) ₃ Ni(bipyrimidyl) ₂] ₂ (BF ₄) ₂	5.081	90.61	87.10	31
[(Tp)Fe ^{III} (CN) ₃ Ni(phen) ₂] ₂ (ClO ₄) ₂	5.086-5.116	91.03	88.60	31
[(pzTp)Fe(CN) ₃ Ni(dpa)](ClO ₄) ₂	5.089-5.100	93.18	85.36	25
[(Tp)Fe(CN) ₃ Ni(dmphen) ₂] ₂ (ClO ₄) ₂	5.166-5.170	86.58	88.26	30
[(pzTp)Fe(CN) ₃ Ni ^{II} (dmphen) ₂] ₂ (ClO ₄) ₂	5.150-5.168	86.28	88.79	30
[(Tp*)Fe ^{III} (CN) ₃ Ni(DMF) ₄] ₂ (OTf) ₂	5.249-5.255	93.81	84.98	27
[(MeTp)Fe(CN) ₃ Ni(tren)] ₂ (ClO ₄) ₂	5.047-5.153	92.00	86.66	33
[(i-BuTp)Fe(CN) ₃ Ni(tren)] ₂ (ClO ₄) ₂	5.047-5.189	89.91	88.08	33
[(Tp*)Fe(CN) ₃ Ni(bipy) ₂] ₂ (OTf) ₂	5.077-5.097	95.07	83.76	28
[TpFe(CN) ₃ Ni(L ¹) ₂] ₂ (ClO ₄) ₂	5.117-5.126	93.17	87.08	29
[(i-BuTp)Fe(CN) ₃ Ni(L ²) ₂] ₂ (ClO ₄) ₂	5.120-5.134	91.45	87.13	29

Abbreviations used for the ligands: Tp = hydrotris(pyrazol-1-yl)borate; tren = tris(2-aminoethyl)amine; bipy = 2,2'-bipyridine; Tp* = hydrotris(3,5-dimethylpyrazolyl)borate); 4-Clbpy = 4-chlorine-2,2'-dibipyridine; phen = 1,10-phenanthroline; pzTp = tetrakis(pyrazol-1-yl)borate; dpa = 2,2'-dipyridyl amine; dmphen = 2,9-dimethyl-1,10-phenanthroline; MeTp = methyltris(pyrazolyl)borate; OTf = trifluoromethanesulfonate; PhTp = tris(pyrazolyl)phenylborate; i-BuTp = 2-methylpropyltris(pyrazolyl)borate; L¹ = 4,5-[1',4']dithiino[2',3'-b]quinoxaline-2-bis(2-pyridyl)methylene-1,3-dithiole; L² = dimethyl-2-[di(pyridin-2-yl)methylene]-1,3-dithiole-4,5-dicarboxylate.

Table S6: Selected magneto-structural data for heterometallic tetranuclear Fe^{III}-(μ-CN)-Ni^{II} square complexes

Compounds	$\chi_M T$ (a/b) at RT	Max $\chi_M T$	M_S ($\mu\beta$)	g	J/K	Ref.
[Fe(bbp)(CN) ₃ Ni(tpa)] ₂	3.44 a	5.90 a	5.60	2.2	5.92	This work
[(Tp)Fe(CN) ₃ Ni(tren)] ₂ (ClO ₄) ₂	3.57 b	5.69 b	4.97	2.22	6.4	26
[(Tp)Fe(CN) ₃ Ni(bipy) ₂] ₂ [(Tp)Fe(CN) ₃] ₂	6.81 b	208.6 b	9.52	2.67	10.5	26
[Fe(bbp)(CN) ₃ Ni(tren)] ₂	3.52 a	5.24 a	6.34	2.23	4.4	22
[(Tp*)Fe ^{III} (CN) ₃ Ni(4-Clbpy) ₂] ₂	3.28 a	10.60 a	3.84	2.07	6.7	32
[(Tp*)Fe ^{III} (CN) ₃ Ni(bipyrimidyl) ₂] ₂ (BF ₄) ₂	3.54 a	13.89 a	6.32	2	-	31
[(Tp)Fe ^{III} (CN) ₃ Ni(phen) ₂] ₂ (ClO ₄) ₂	3.63 a	6.55 a	6.46	2	-	31
[(pzTp)Fe(CN) ₃ Ni(dpa)](ClO ₄) ₂	3.28 a	9.60 a	6.48	2.23	10.1	25
[(Tp)Fe(CN) ₃ Ni(dmphen) ₂] ₂ (ClO ₄) ₂	4.09 a	8.26 a	6.55	2.30-2.21	30.7-27.0	30
[(pzTp)Fe(CN) ₃ Ni ^{II} (dmphen) ₂] ₂ (ClO ₄) ₂	3.72 a	13.03 a	6.60	2.39- 2.20	24.4-17.9	30
[(Tp*)Fe ^{III} (CN) ₃ Ni(DMF) ₄] ₂ (OTf) ₂	4.1 b	8.27 b	6.11	2.20	7.6	27
[(PhTp)Fe(CN) ₃ Ni(tren)] ₂ (ClO ₄) ₂	3.72 b	6.97 b	5.84	2.284	6.0	33
[(MeTp)Fe(CN) ₃ Ni(tren)] ₂ (ClO ₄) ₂	3.76 b	5.98 b	5.19	2.305	4	33
[(i-BuTp)Fe(CN) ₃ Ni(tren)] ₂ (ClO ₄) ₂	3.76 b	7.25 b	5.66	2.285	7.8	33
[(Tp*)Fe(CN) ₃ Ni(bipy) ₂] ₂ (OTf) ₂	3.8 a	7.7 a	6.00	2.29	9.4	28
[TpFe(CN) ₃ Ni(L ¹) ₂] ₂ (ClO ₄) ₂	3.34 b	5.79	4.40	2.14	6.1	29
[(i-BuTp)Fe(CN) ₃ Ni(L ²) ₂] ₂ (ClO ₄) ₂	3.35 b	6.14	4.32	2.14	6.0	29

*Where, a=cm³ mol⁻¹ K & b = emu mol⁻¹ K, M= Magnetization, H= Magnetic Field, J= exchange interaction.

Table S7: Electrochemical results of compound **1**, **2** & **3**

Complex	$E_{pa}(\text{V})$	$E_{pc} (\text{V})$	$E_{1/2}(\text{V})$	$\Delta E_p(\text{V})$
$\text{K}_2\text{Ni}(\text{CN})_4 \cdot \text{H}_2\text{O}$	-0.63	-0.88	-0.76	0.25
	1.03	0.74	0.89	0.29
$(\text{TBA})_2[\text{Fe}(\text{bbp})(\text{CN})_3]$	-0.63	-0.77	-0.70	0.14
1	0.61	-	-	-
	1.10	-	-	-
	-0.67	-0.95	-0.81	0.28
2	0.94	0.85	0.89	0.09
	0.64	-	-	-
	-0.66	-0.94	-0.8	0.28
3	-0.64	-0.82	-0.73	0.18
	-0.39	-0.56	-0.47	0.18
	-0.16	-0.32	-0.24	0.16
	0.23	0.09	0.16	0.14
3 (after acid addition)	-0.36	-0.55	-0.45	0.19
	0.20	0.10	0.15	0.10
	0.33	0.28	0.30	0.05
	0.49	0.43	0.46	0.06

E_{pa} = oxidative peak potential. E_{pc} = reductive peak potential. $E_{1/2} = (E_{pc} + E_{pa})/2$,

$$\Delta E_p = E_{pa} - E_{pc}.$$

References:

1. X. Jiang, B. Tao, X. Yu, Y. Wang and H. Xia, *RSC Advances*, 2015, **5(25)**, 19034-19040.
2. P. -F. Zhuang, Y. -J. Zhang, H. Zheng, C. -Q. Jiao, L. Zhao, J. -L. Wang, C. He, C.-Y. Duan and T. Liu, *Dalton Trans.*, 2015, **44**, 3393-3398.
3. B. Nowicka, M. Reczyński, M. Rams, W. Nitek, J. Żukrowski, C. Kapusta and B. Sieklucka, *Chem. Commun.*, 2015, **51**, 11485-11488.
4. J. Kim, S. Han, K. I. Pokhodnya, J. M. Migliori and J. S. Miller, *Inorg. Chem.*, 2005, **44(20)**, 6983-6988.